This article has been accepted for inclusion in a future issue of this journal. Content is final as presented, with the exception of pagination.

An Improved Method For Retrieving Land Surface Albedo Over Rugged Terrain

Bo Gao, Li Jia, and Massimo Menenti

***Abstract*—Land surface albedo is a very important parameter, which can be derived from a bidirectional reflectance distribution function (BRDF) model with angular integration of BRDF in a particular distribution of downward solar irradiance. The Algorithm for MODIS Bidirectional Reflectance Anisotropic of Land Surface (AMBRALS) utilizes a kernel-driven BRDF model to retrieve land surface albedo, but it does not take into account the topographic effect. This letter proposed an improved method by adding topographic factor to the AMBRALS, which removes the topographic effect on land surface reflectance and considers the topographic effect in retrieving land surface albedo. This method is applied to the HJ-1A/B CCD land surface reflectance data to retrieve the land surface albedo. The results are compared with those from the AMBRALS and with the ground measurements. The comparison results show that the proposed method performs well in general and better than the AMBRALS over rugged area.**

***Index Terms*—Bidirectional reflectance distribution function (BRDF), digital elevation model (DEM), HJ-1A/B, land surface albedo, topographic effect.**

I. Introduction

AS AN important parameter affecting the Earth's climate, land surface albedo frequently served as an indicator to quantify how much energy the Earth receives from the sun. Land surface albedo can be observed given a particular distribution of downward solar irradiance [1] and is relevant to the directional-hemispherical surface albedo which is driven by the angular integration of bidirectional reflectance distribution function (BRDF).

The Algorithm for MODIS Bidirectional Reflectance Anisotropic of Land Surface (AMBRALS) is an algorithm designed for land surface albedo retrieval using NASA's MODIS data [2]. This algorithm has been widely accepted, but it cannot deal with topographic effect, which leads to large uncertainties in albedo retrieval over rugged terrain. To overcome this shortage, we attempt to introduce a topographic factor into the AMBRALS to deal with topographic effect.

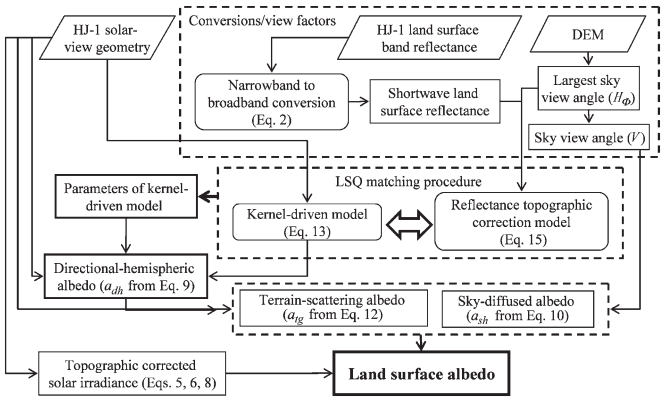

Fig. 1. Flowchart of the improved method to retrieve land surface albedo.

The topography plays different roles in the retrieval of land surface albedo at different spatial scales. At high spatial resolution, topography results in multiscattering among pixels and varies the downward solar irradiance. At low spatial resolution, topography leads to multiscattering and obscuration within pixel. A hypothesis is made that a digital elevation model (DEM) with horizontal resolution of 30 m could fully capture the topographic characteristics. In a 30 m grid, the topography modifies the solar reflecting geometry [3] and influences land surface albedo in several ways: 1) varying the downward direct solar radiance; 2) affecting downward diffuse radiance; and 3) modifying the reflected radiance due to non-flat surface [4].

This letter proposed an improved method to retrieve land surface albedo over rugged terrain. The results from this algorithm are compared with those from AMBRALS. Discussions and further objectives are given in the Summary.

II. Method

The following provides an algorithm outline for the derivation of BRDF and albedo from atmospherically and topographically corrected multi-angular reflectance observations in rugged terrain. This method (hereafter referred to "improved method") is developed by performing topographic correction to the AMBRALS (referred to "MODIS method").

The improved method utilizes HJ-1A/B CCDs land surface reflectance to retrieve the land surface albedo (Fig. 1) and includes the following three steps. First, topographic correction for land surface reflectance as driving data retrieving the

Manuscript received February 15, 2013; revised June 28, 2013; accepted July 9, 2013. This work was supported in part by the CAS/SAFEA International Partnership Program for Creative Research Teams under Grant KZZD-EW-TZ-09, the EU-FP7 project CEOP-AEGIS under Grant 212921, and the strategic research program KBIV "Sustainable spatial development of ecosystems, landscapes, seas and regions" which is funded by the Dutch Ministry of Economic Affairs, and carried out by Wageningen University and Research Centre. *(Corresponding author: L. Jia.)*

B. Gao is with the State Key Laboratory of Remote Sensing Science, Jointly Sponsored by the Institute of Remote Sensing and Digital Earth of Chinese Academy of Sciences and Beijing Normal University, Beijing 100101, China.

L. Jia is with the State Key Laboratory of Remote Sensing Science, Jointly Sponsored by the Institute of Remote Sensing and Digital Earth of Chinese Academy of Sciences and Beijing Normal University, Beijing 100101, China and also with the Alterra, Wageningen University and Research Centre, Wageningen, The Netherlands (e-mail: li.jia@wur.nl).

M. Menenti is with the Delft University of Technology, 2628 CN Delft, The Netherlands and also with the State Key Laboratory of Remote Sensing Science, Jointly Sponsored by the Institute of Remote Sensing and Digital Earth of Chinese Academy of Sciences and Beijing Normal University, Beijing 100101, China.

Color versions of one or more of the figures in this paper are available online at http://ieeexplore.ieee.org.

Digital Object Identifier 10.1109/LGRS.2013.2275072

1545-598X © 2013 IEEE

This article has been accepted for inclusion in a future issue of this journal. Content is final as presented, with the exception of pagination.

TABLE I
WEIGHTS FOR CONVERTING BAND ALBEDO TO SHORTWAVE ALBEDO [6]

Band	1	2	3	4
HJ1ACCD1	-0.5878	0.6543	0.4183	0.3891
HJ1ACCD2	-0.5138	0.5175	0.4838	0.3865
HJ1BCCD1	-0.6066	0.6175	0.4703	0.3925
HJ1BCCD2	-0.5149	0.5403	0.4592	0.3898

parameters of BRDF is done. The DEM and MODTRAN are used to calculate the distribution of surface solar irradiance integration. Second, combining with the DEM data, we retrieve the directional-hemispherical albedo, the sky-diffused albedo, and the terrain-scattering albedo in rugged terrain. The land surface albedo is finally calculated by the linear composition of directional-hemispherical albedo, sky-diffused albedo and terrain-scattering albedo weighted by the components of direct solar, sky-diffused, and terrain-scattering irradiance.

Land surface albedo is the fraction of incoming shortwave energy reflected by the land surface. By definition, land surface albedo can be expressed as (1), shown at the bottom of the page, where $R(\theta_i, \theta_v, \Phi_i, \Phi_v, \lambda)$ is the bidirectional reflectance factor (BRF) of a pixel, $E(\theta_i, \Phi_i, \lambda)$ is the downward solar radiance, θ_i is the sun zenith, θ_v is the view zenith, Φ_i is the sun azimuth, Φ_v is the view azimuth, and λ is the wavelength.

The spectral (or band) albedo $\alpha(\lambda)$ can be written as (2), shown at the bottom of the page.

Considering the spectral range of a sensor, we can get the shortwave (0.4–2.5 μm) albedo from the in-band albedo [5]

$$a_{shortwave} = \sum_j w_j a_j(\lambda) \tag{3}$$

where w_j is the weight of band j. Table I gives the weights of HJ-1A/B bands used to convert band reflectance to shortwave broad band reflectance [6]. Similar method is used in MODIS products (MCD43B1). In the following text of the letter, the term "albedo" is meant broadband albedo in shortwave range and the subscript "shortwave" is removed.

Land surface albedo over rugged terrain can be defined as:

$$\alpha = \frac{F_{dir}a_{dh} + F_{ref}a_{th} + F_{dif}a_{sh}}{F_{dir} + F_{ref} + F_{dif}} \tag{4}$$

where F_{dir} is the direct solar irradiance to slope, F_{ref} is the terrain-scattering irradiance from neighbor pixels, F_{dif} is the diffused solar irradiance on the slope, a_{th} is terrain-scattering albedo, a_{dh} is directional-hemispheric albedo, and a_{sh} is sky-diffused albedo.

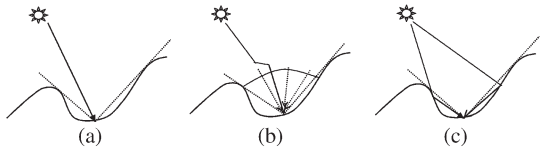

Fig. 2. Downward solar irradiance: (a) direct solar irradiance; (b) diffused solar irradiance; and (c) terrain-scattering irradiance from the adjacent terrain.

A. Downward Solar Irradiance Distribution Over Rugged Terrain

Over rugged terrain, the temporal and spatial distribution of surface solar irradiance is a result of complex interactions among the incoming solar beam, the atmosphere, and the surface. The downward solar irradiance over rugged terrain includes: direct solar irradiance, diffused solar irradiance, and terrain-scattering irradiance from the adjacent terrain (Fig. 2).

The direct solar irradiance and the diffused solar irradiance can be simulated by MODTRAN [7]. The direct solar irradiance F_{dir} on the slope of a target pixel can be expressed as

$$F_{dir} = \Theta E \cos i \tag{5}$$

where Θ is a binary value, Θ is 0 for the slope in shadow, otherwise it is l; E is the direct solar irradiance at the bottom of atmosphere (BOA); i is the angle between solar incidence and the normal of the slope.

The diffused solar irradiance F_{dif} on the slope of a target pixel can be expressed as:

$$F_{dif} = E_{dif}V \tag{6}$$

where E_{dif} is the diffuse solar irradiance over flat surfaces, V is the sky view factor which is the ratio of the diffuse sky irradiance at a point to that on an unobstructed horizontal surface. V on slope S with aspect A is found by integrating over the unobstructed hemisphere above a target pixel (i.e., from the zenith downward to the local horizon) through angle H_ϕ for each azimuth angle Φ [12]

$$V = \frac{1}{2\pi}\int_0^{2\pi} \left[\cos S \sin^2 H_\phi + \sin S \cos(\phi - A)(H_\phi - \sin H_\phi \cos H_\phi)\right] d\phi \tag{7}$$

where H_ϕ is the largest sky view angle in the azimuth direction ϕ. For a fully unobstructed horizontal surface $H_\phi = \mathrm{pi}/2$. The horizon of the target pixel is the consequence of either the "self-shadowing" by the slope itself or the adjacent ridge [Fig. 3(a)].

$$a_{shortwave} = \frac{\int_{0.4\ \mu\mathrm{m}}^{2.5\ \mu\mathrm{m}} \int_0^{2\pi} \int_0^{\frac{\pi}{2}} \int_0^{2\pi} \int_0^{\frac{\pi}{2}} E(\theta_i, \phi_i, \lambda) R(\theta_i, \theta_v, \phi_i, \phi_v, \lambda) \cos\theta_v \sin\theta_v \cos\theta_i \sin\theta_i d\theta_v d\phi_v d\theta_i d\phi_i d\lambda}{\pi \int_{0.4\ \mu\mathrm{m}}^{2.5\ \mu\mathrm{m}} \int_0^{2\pi} \int_0^{\frac{\pi}{2}} E(\theta_i, \phi_i, \lambda) \cos\theta_i \sin\theta_i d\theta_i d\phi_i d\lambda} \tag{1}$$

$$a(\lambda) = \frac{\int_0^{2\pi} \int_0^{\frac{\pi}{2}} \int_0^{2\pi} \int_0^{\frac{\pi}{2}} E(\theta_i, \phi_i, \lambda) R(\theta_i, \theta_v, \phi_i, \phi_v, \lambda) \cos\theta_v \sin\theta_v \cos\theta_i \sin\theta_i d\theta_v d\phi_v d\theta_i d\phi_i}{\pi \int_0^{2\pi} \int_0^{\frac{\pi}{2}} E(\theta_i, \phi_i, \lambda) \cos\theta_i \sin\theta_i d\theta_i d\phi_i} \tag{2}$$

This article has been accepted for inclusion in a future issue of this journal. Content is final as presented, with the exception of pagination.

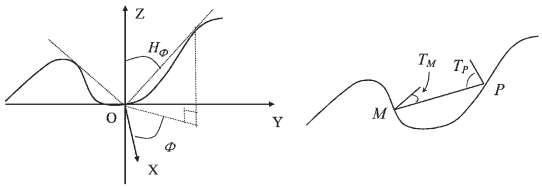

Fig. 3. (a) Largest sky view angle H_Φ in the direction Φ, OXY is horizontal plane, OZ is perpendicular of OXY; and (b) Parameters used for calculating terrain-scattering irradiance.

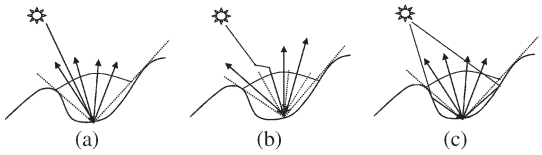

Fig. 4. Description of land surface albedo in rugged terrain: (a) directional hemispheric albedo; (b) sky-diffused albedo; and (c) terrain-scattering albedo.

The terrain-scattering irradiance is calculated using the method of Proy *et al.* [8]. Assuming the surface is Lambertian and the target pixel M is in the center of a subset of 5×5 pixels matrix and pixel P as one of the neighboring pixels of the target pixel M, the reflected irradiance from each surrounding point P to the pixel M, F_{ref}, can be calculated as:

$$F_{ref} = \sum_{p=1}^{N} \frac{L_p \cos T_M \cos T_P dS_p}{r_{mp}^2} \Theta' \tag{8}$$

where L_p is the radiance received by the target pixel that comes from the neighboring pixel, T_p is the angle between the line MP and the normal of the target pixel, T_M is the angle between the line MP and the normal of surrounding pixel [Fig. 3(b)], dS_p is the area of the target pixel, and r_{mp} is the length from surrounding pixel to target pixel. Θ' is 1 if surrounding pixel P and M is unobstructed, otherwise is 0.

B. Albedo by Integration of the BRDF Based on Downward Solar Irradiance Distribution Over Rugged Terrain

Over a horizontally flat surface, land surface albedo retrieved from satellites is usually composed of directional-hemispheric albedo (black-sky albedo) and bi-hemispheric albedo (white-sky albedo). Over rugged terrain, as mentioned in (4), the land surface albedo is a linear weighted composition of directional-hemispheric albedo, sky-diffused albedo, and terrain-scattering albedo (Fig. 4). Directional-hemispheric albedo, a_{dh}, is given by

$$a_{dh}(\theta_i, \phi_i) = \frac{1}{\pi} \int_0^{2\pi} \int_0^{\frac{\pi}{2}} R(\theta_i, \theta_v, \phi_i, \phi_v) \cos\theta_v \sin\theta_v d\theta_v d\phi_v \tag{9}$$

where R is BRF of land surface, a function of sun and viewing angles, and its inversion from the terrain-corrected land surface reflectance of satellite observations is given in Section II-C.

Sky-diffused albedo over rugged terrain, a_{sh}, is defined as

$$a_{sh} = \frac{\int_0^{2\pi} \int_0^{Hm} a_{dh}(\theta_i, \phi_i) \cos\theta_i \sin\theta_i d\theta_i d\phi_i}{\int_0^{2\pi} \int_0^{Hm} \cos\theta_i \sin\theta_i d\theta_i d\phi_i} \tag{10}$$

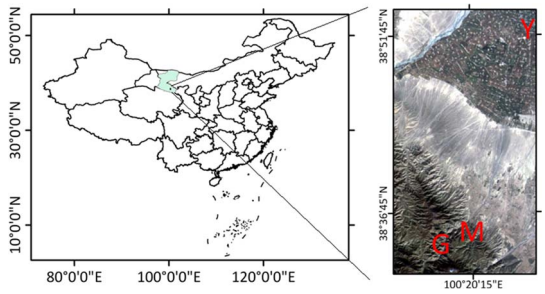

Fig. 5. Three experimental sites of the WATER project in the Heihe River basin shown on true color image of HJ-1B CCD1 band3, band2, and band1 on September 28th, 2009: G for Guantan, M for Maliantan and Y for Yingke.

where Hm is the mean value of H_ϕ. For simplicity, we make the hypothesis that H_ϕ is symmetric so that

$$Hm = V * \pi/2. \tag{11}$$

Terrain-scattering albedo, a_{th}, is defined as

$$a_{th} = \frac{\int_0^{2\pi} \int_{Hm}^{\frac{\pi}{2}} a_{dh}(\vartheta_i, \phi_i) \cos\vartheta_i \sin\vartheta_i d\vartheta_i d\phi_i}{\int_0^{2\pi} \int_{Hm}^{\frac{\pi}{2}} \cos\vartheta_i \sin\vartheta_i d\vartheta_i d\phi_i}. \tag{12}$$

C. Kernel-Driven BRDF Model and Inversion Using Land Surface Reflectance by Topography Correction

In (9), a kernel-driven BRDF model is adopted to calculate the BRDF which is a linear composite of three kernels [9], i.e., the isotropic scattering, the volume scattering, and geometric optics scattering

$$R(\theta_i, \theta_v, \phi_i, \phi_v)/\pi = f_{iso} + f_{vol} k_{vol}(\theta_i, \theta_v, \phi_i, \phi_v) + f_{geo} k_{geo}(\theta_i, \theta_v, \phi_i, \phi_v) \tag{13}$$

where the volume scattering term k_{vol} is from Ross-Thick kernel [10], the geometrical optical scattering term k_{geo} is from Li-SparseR kernel [11]. f_{vol} is the coefficient of k_{vol}, f_{geo} is the coefficient of k_{geo}, f_{iso} is the coefficient of isotropic term.

Given the topographically and atmospherically corrected reflectance $\rho_{top-obs}$ at an angle $(\theta_i, \theta_v, \Phi_i, \Phi_v)$, analytical solutions for the model parameters f_k are obtained by minimization of a least-squares error function $(\partial e^2/\partial f_k = 0)$

$$e^2 = 1/d \sum_l \left(\rho_{top-obs}(\theta_{il}, \theta_{vl}, \phi_{il}, \phi_{vl}) - R(\theta_{il}, \theta_{vl}, \phi_{il}, \phi_{vl})\right)^2 \tag{14}$$

where l is number of observations and d is degree of freedom.

According to Doizer's work [12], the topography may change sky-diffused irradiance and enhance the scattering radiation from surrounding pixels. To remove the topographic influence, a simple topographic correction physical model is used to remove topographic influence on the BOA reflectance [13]

$$\rho_{top-obs}(\theta_{il}, \theta_{vl}, \phi_{il}, \phi_{vl}) = \pi \frac{r_{obs} - F_{ref}\left(\frac{r_{obs}}{F_{dir}}\right)}{F_{dir}} \tag{15}$$

where r_{obs} is the radiance reflected by land surface in viewing direction after atmospheric correction at the BOA. Here, the reflected sky diffused irradiance is neglected, as it is a very small fraction compared to the enhanced terrain scattering on a sunny day.

This article has been accepted for inclusion in a future issue of this journal. Content is final as presented, with the exception of pagination.

TABLE II
PARAMETERS OF HJ-1A/B

Satellite	Band	Spectral (μm)	Spatial resolution (m)
HJ-1A/1B	1	0.43 ~ 0.52	30
	2	0.52 ~ 0.60	30
	3	0.63 ~ 0.69	30
	4	0.76 ~ 0.90	30

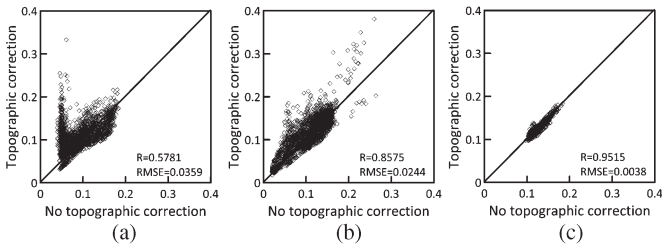

Fig. 6. Comparison between the land surface reflectance with topographic correction and the one without topographic correction on Sept 14th, 2009 at (a) Guantan, (b) Maliantan, and (c) Yingke.

III. STUDY AREA AND DATA

Three sites located in Heihe river basin in northwestern (Fig. 5) China are selected as the study area: they are Yingke (grassland, flat, mean slope is 2°), Maliantan (grassland, mountain, mean slope is 14°), and Guantan (forest, mountain, mean slope is 20°). The slope is calculated as the angle between the horizontal plane and the slope plane. Ground measurements in these sites used for preliminary validation were collected during the WATER project [14]. Radiance data from Chinese satellite HJ-1A/B from 1st Sep, 2009 to 30th Nov, 2009 are collected. HJ-1A/B carries two CCDs of which have four bands in shortwave range (Table II) with revisit period as one or two days. The ASTER Global Digital Elevation Model (GDEM) with 30 m spatial resolution is used for calculating topographic parameters, i.e., slope and aspect by ATCOR software.

IV. RESULTS

An experiment was done by applying the method described in Section II to the data introduced in Section III. Preliminary results are given below.

A. Topographic Correction of Land Surface Reflectance

Topographic correction is applied to the atmospherically corrected reflectance from HJ-1. Fig. 6 shows the comparison between the topographic corrected reflectance and non-topographic corrected reflectance. It is obvious that in Guantan and Maliantan, the topographic effect is more significant, so the difference in land surface reflectance between before and after topographic correction is larger than that for Yingke (Fig. 6). Obviously, the more rugged the terrain is, the better the effect of correction is.

B. Albedo From Improved Method and MODIS Method

Land surface albedo varies with the change of downward solar radiation distribution. Over rugged terrain, downward solar radiation is greatly anisotropic comparing to that over a flat area. As such, over rugged terrain, the anisotropy of the downward solar irradiance should be taken into account for calculating the albedo by integral of BRDF. Thus, if the rugged terrain is steeper, the land surface albedo differs more from that of a flat area.

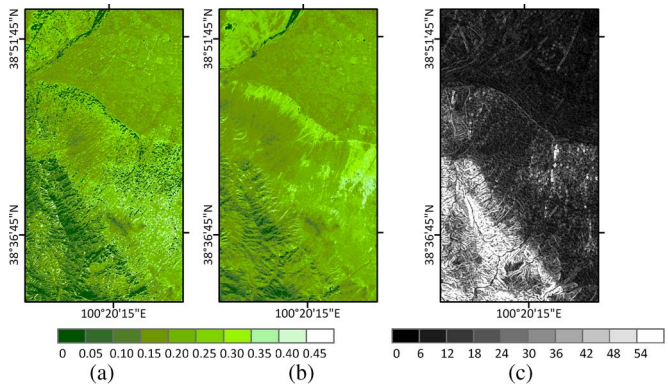

Fig. 7. Retrieved albedo by (a) the improved method and (b) the MODIS method, using HJ-1A/B CCDs 8 days land surface reflectance from October 24th to November 10th, 2009. (c) The slope [0, 90°].

The improved method (Section II) that considers the topographic effect is built to retrieve the land surface albedo using the data selected on the sunny days mentioned in Section III. Retrieval is also done by the MODIS method using the same data. The results are shown in Fig. 7. The pixels with water and singular retrievals are masked as zero value. In the study area, the slope increases [Fig. 7(c)] from northeast to southwest; consequently, the results of the albedo from the two methods are very similar in the northeast, while they are significantly different in the southwest [Fig. 7(a) and (b)].

C. Comparing the Improved Method and MODIS Method at Three Sites

Fig. 8 shows the inversion results of three subsets (1.5 km × 1.5 km) surrounding the three experimental sites by applying the HJ-1 data between Oct 24th, 2009 to Nov 10th, 2009 to the two methods, i.e., the MODIS method and the improved method. Both of the Maliantan site and the Guantan site have rugged slope, while Yingke is very flat. Guantan is slightly more rugged than Maliantan.

Large difference in spatial pattern is found at Guantan and Maliantan subsets in the retrieved land surface albedo between using MODIS [Fig. 8(a) and (b)] and the improved method [Fig. 8(d) and (e)] over mountain areas in particular over large slope pixels. On the contrary, in Yingke subset, the two results are very similar. This is because the slopes in the subsets of Maliantan and Guantan are steeper than that of Yingke subset. More gaps are seen in the results from the improved method over pixels with deep slopes. This is because, in addition to singular retrieval, the retrieval is terminated over these pixels since magnitude of solar direct irradiance received by the surface of these pixels is insufficient to drive the model and these pixels are masked out.

Furthermore, the quantitative comparison of the two methods is shown in Fig. 9 by scattering plot of the two results in Fig. 8. In theory, the difference between the results of the two methods is more obvious when the terrain is more rugged. This is approved by the results shown in Fig. 9; it is apparent that the topographic effect is obvious for Maliantan and Guantan subsets where topography is steeper, while not obvious for Yingke subset where the land surface is flat.

This article has been accepted for inclusion in a future issue of this journal. Content is final as presented, with the exception of pagination.

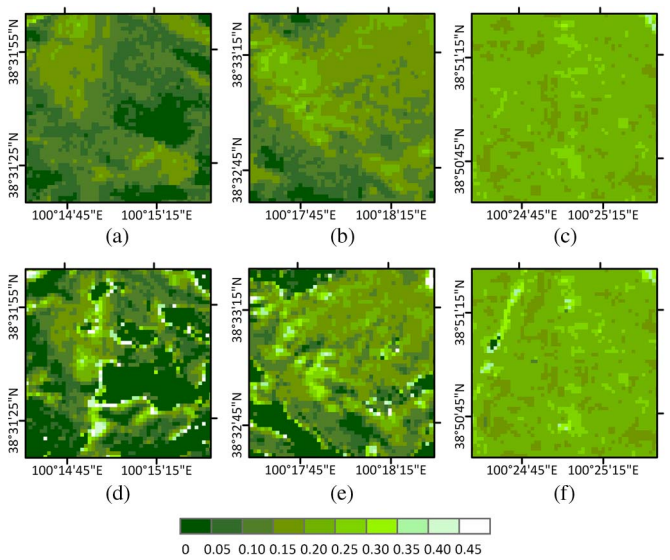

Fig. 8. Retrieved land surface albedo: (a) Guantan, (b) Maliantan, (c) Yingke using MODIS method and (d) Guantan, (e) Maliantan, (f) Yingke using the improved method, respectively. (1.5 km × 1.5 km subset of same data as in Fig. 7 with each site centered in the middle. Pixels with water and singular retrievals are masked as zero).

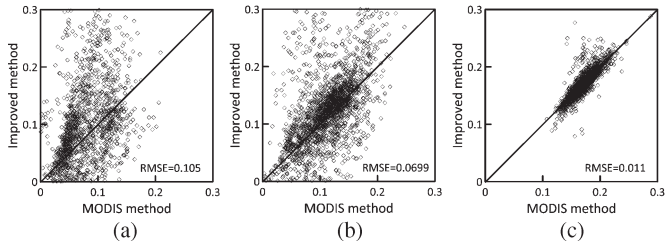

Fig. 9. Comparison of the retrieved land surface albedo using MODIS and the improved method in a 1.5 km × 1.5 km subset of each one of the three sites at: (a) Guantan; (b) Maliantan; and (c) Yingke.

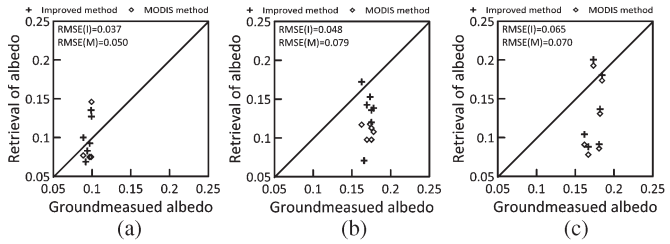

Fig. 10. Comparison of results from two methods at: (a) Guantan, (b) Maliantan, (c) Yingke. RMSE (I): for improved method, RMSE (M): for MODIS method.

Dealing with topographic effect, the improved method is more advanced than the MODIS method. First, the improved method corrects the topographic effect for land surface reflectance. Second, by considering anisotropy of the downward solar irradiance over rugged terrain, we can calculate the land surface albedo as the linear composition of the three albedo contributions. The MODIS method does not take the topographic effect into account to retrieve the albedo.

The results driven by the HJ-1A/B land surface reflectance from September 1st to November 30th in 2009 are compared with ground measurements at the three sites: Guantan, Maliantan, and Yingke (Fig. 10).

This comparison illustrates that the improved method, to a certain extent, corrects the topographic effect effectively. The effect is inapparent at the Yingke site, while the correction at Maliantan site and Guantan site is more obvious.

That is to say, if the topography is more complex, the corrected results for the topography are better.

V. Summary

An improved method is developed to calculate the land surface albedo accurately. The calculated results are compared with in situ measurements, which verifies that the improved method has a better accuracy in particular in rugged terrain. There are still some unresolved issues: 1) a better validation with a longer period of ground measurements should be verified in the near future; 2) the topographic correction for land surface reflectance in this work, to some extent, has corrected the effect of terrain. However, the method did not consider the correction on land surface reflectance in obstructed pixels; this work will be processed in further study.

References

[1] S. Liang, A. H. Strahler, and C. Walthall, "Retrieval of land surface albedo from satellite observations: A simulation study," *J. Appl. Meteorol.*, vol. 38, no. 6, pp. 712–725, 1999.

[2] W. Lucht, C. B. Schaaf, and A. H. Strahler, "An algorithm for the retrieval of albedo from space using semiempirical BRDF models," *IEEE Trans. Geosci. Remote Sens.*, vol. 38, no. 2, pp. 977–998, Mar. 2000.

[3] C. B. Schaaf, X. Li, and A. H. Strahler, "Topographic effects on bidirectional and hemispherical reflectances calculated with a geometric-optical canopy model," *IEEE Trans. Geosci. Remote Sens.*, vol. 32, no. 6, pp. 1186–1193, Nov. 1994.

[4] Y. Chen, A. Hall, and K. N. Liou, "Application of three-dimensional solar radiative transfer to mountains," *J. Geophys. Res.—Atmos.*, vol. 111, no. D21, Nov. 2006.

[5] S. Liang, "Narrowband to broadband conversions of land surface albedo I Algorithms," *Remote Sens. Environ.*, vol. 76, no. 2, pp. 213–238, 2001.

[6] S. Liu, "The angular & spectral kernel BRDF model for albedo retrieval," Ph.D. dissertation, Univ. Chinese Acad. Sci., Beijing, China, 2010.

[7] P. Acharya, A. Berk, L. Bernstein, M. Matthew, S. Adler-Golden, D. Robertson, G. Anderson, J. Chetwynd, F. Kneizys, E Shettle, L. Abreu, W. Gallery, J. Selby, and S. Clough, *MODTRAN user's manual versions 3.7 and 4.0*. Bedford, MA, USA: Air Force Research Laboratory, Space Vehicles Directorate, Hanscom Air Force Base, 1998.

[8] C. Proy, D. Tanre, and P. Y. Deschamps, "Evaluation of topographic effects in remotely sensed data," *Remote Sens. Environ.*, vol. 30, no. 1, pp. 21–32, Oct. 1989.

[9] W. Wanner, X. Li, and A. H. Strahler, "On the derivation of kernels for kernel-driven models of bidirectional reflectance," *J. Geophys. Res.—Atmos.*, vol. 100, no. D10, pp. 21077–21089, Oct. 1995.

[10] J. L. Roujean, "A bidirectional reflectance model of the Earth's surface for the correction of remote sensing data," *J. Geophys. Res.*, vol. 97, no. D18, pp. 20455–20468, Dec. 1992.

[11] X. Li and A. H. Strahler, "Geometric-optical bidirectional reflectance modeling of the discrete crown vegetation canopy—Effect of crown shape and mutual shadowing," *IEEE Trans. Geosci. Remote Sens.*, vol. 30, no. 2, pp. 276–292, Mar. 1992.

[12] J. Dozier and J. Frew, "Rapid calculation of terrain parameters for radiation modeling from digital elevation data," *IEEE Trans. Geosci. Remote Sens.*, vol. 28, no. 5, pp. 963–969, Sep. 1990.

[13] R. Dubayah, "Estimating net solar-radiation using landsat thematic mapper and digital elevation data," *Water Resour. Res.*, vol. 28, no. 9, pp. 2469–2484, Sep. 1992.

[14] X. Li, X. Li, Z. Li, M. Ma, J. Wang, Q. Xiao, Q. Liu, T. Che, E. Chen, G. Yan, Z. Hu, L. Zhang, R. Chu, , P. Su, Q. Liu, S. Liu, J. Wang, Z. Niu, Y. Chen, R. Jin, W. Wang, Y. Ran, X. Xin, and H. Ren, "Watershed allied telemetry experimental research," *J. Geophys. Res.—Atmos.*, vol. 114, no. D22103, pp. 1–19, Nov. 2009.